Simultaneous AFM and STM measurements on the Si(111)-(7×7) surface

Yoshiaki Sugimoto,* Yuuki Nakajima, Daisuke Sawada, Ken-ichi Morita, Masayuki Abe, and Seizo Morita
Graduate School of Engineering, Osaka University, 2-1, Yamada-Oka, Suita, Osaka 565-0871, Japan
(Received 25 February 2010; published 29 June 2010)

We perform simultaneous atomic force microscopy (AFM) and scanning tunneling microscopy (STM) measurements on the Si(111)-(7×7) surface. AFM/STM constant height images are obtained at various tip-surface distances. Force/current distance spectroscopy using the same tip apex allows us to estimate the relative tip-surface distance for each image as well as the short/long-range force and the tunneling current. We demonstrate that the tunneling current at tip-surface distances where AFM clearly resolves atoms is much larger than the typical values in conventional STM. In addition, at the tip-surface distances for conventional STM, the short-range force is too small to provide atomic contrast in AFM. We show that the differences in the signal-to-noise ratio of the constant height images between AFM and STM produce different optimal imaging distances. In addition, we note that the different imaging distance also influences images obtained using double tips.

DOI: 10.1103/PhysRevB.81.245322 PACS number(s): 68.37.Ps, 68.37.Ef, 68.47.Fg, 68.35.bg

I. INTRODUCTION

Atomic force microscopy (AFM), operated using a frequency-modulation technique, has been developed as a powerful tool for surface physics, surface chemistry, and nanotechnology.[1,2] In this method, a cantilever is oscillated at its resonance frequency (f_0), and the frequency shift (Δf) caused by the interaction force between the tip and sample (F) is detected.[3] Using this technique, true atomic resolution can be routinely obtained not only in ultrahigh vacuum but also in air and liquid environments.[4] Since the imaging principle of AFM is different from that of scanning tunneling microscopy (STM), these two techniques provide complementary information on surfaces at the single atomic level. The image contrast in STM, in which the tunneling current (I_t) is observable, reflects the local density of state (LDOS) of electrons near the Fermi level, while the AFM image contrast reflects the F field related to electronic states with a wider energy range.

I_t can be simultaneously measured during AFM operation when a bias voltage (V_s) is applied between the conductive tip and the sample. When the bandwidth of a current-to-voltage converter is much smaller than f_0, the time-averaged tunneling current ($\langle I_t \rangle$) is observed. From the early period of the development of noncontact AFM, simultaneous operation of AFM and STM has been reported. There are two ways in which AFM/STM simultaneous measurements can be carried out, as shown in Fig. 1. The topographic mode, wherein the tip-surface distance is regulated by Δf or $\langle I_t \rangle$, has been widely used, see Fig. 1(a). Some groups obtained topographic images regulated by Δf while simultaneously recording $\langle I_t \rangle$ (Refs. 5 and 6) while others obtained topography regulated by $\langle I_t \rangle$ with simultaneous recording of Δf.[7–10] In these methods, however, one cannot separate the AFM and STM information because of cross-talk between Δf and $\langle I_t \rangle$ signals. For example, when $\langle I_t \rangle$ is used for the tip-surface regulation, artificial atomic contrast can appear in the Δf image. The long-range force that is modulated by changing the tip-surface distance contributes to Δf contrast even at a far distance where the short-range force is too small to produce true atomic resolution in AFM. Therefore, constant height operation of the AFM/STM is necessary to measure the Δf and $\langle I_t \rangle$ signals independently. In this mode, Δf and $\langle I_t \rangle$ are recorded during the tip scanning on the surface at constant height with the feedback loop for maintaining the tip-surface distance opened, see Fig. 1(b). A few groups have reported constant height AFM/STM using quartz tuning forks at cryogenic temperatures where the thermal drift is negligibly small.[11–14] On the other hand, we have demonstrated simultaneous AFM/STM at constant height even at room temperature by using a feed-forward technique for compensation of the thermal drift.[15] The measurements using metal-coated Si cantilevers produced clear atomic contrasts in the Δf and $\langle I_t \rangle$ images. It has also been demonstrated that the chemical bonding force and LDOS can be measured above a specific site using the same tip apex. Nevertheless, the differences between AFM and STM, such as the optimal tip-surface distance for obtaining atomic resolution and the signal-to-noise ratio in their observables, have not been perfectly clarified.

In this paper, we investigate the difference in the optimal tip-surface distance to obtain atomic resolution between AFM and STM. Δf and $\langle I_t \rangle$ were simultaneously recorded on the Si(111)-(7×7) surface with constant height tip scanning at various tip-surface distances. To obtain the relative tip-surface distance for each image, the tip-surface distance dependence of Δf and $\langle I_t \rangle$ [$\Delta f(z)$ and $\langle I_t(z) \rangle$] were simulta-

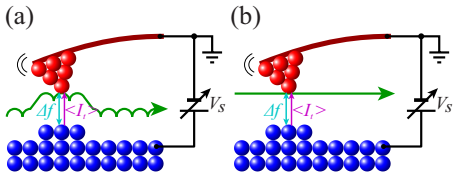

FIG. 1. (Color online) A schematic model of AFM/STM simultaneous measurements in the (a) topographic mode and (b) constant height mode. In the topographic mode, the tip-surface distance is regulated using Δf and recording $\langle I_t \rangle$ or vice versa. In the constant height mode, Δf and $\langle I_t \rangle$ are simultaneously measured at constant height scan without feedback control of the tip-surface distance.

neously measured using the same tip state as used for imaging. To shed some light on the difference in the optimal distance between AFM and STM, the signal-to-noise ratio in the constant height AFM/STM images are discussed. In addition, we show that the difference in optimal distance also influences the contrast in the AFM/STM images accounted for by the double tip effect. We note that single AFM operation is not sufficient to identify tip apex atoms that mediate the tunneling current.

The remainder of the present paper is organized as follows. The conversion formulas between Δf ($\langle I_t \rangle$) and F (I_t) are described in Sec. II. We present the experimental method used in Sec. III. Results and discussion are presented in Sec. IV. In Sec. IV A, we show the combination experiments of constant height AFM/STM imaging and $\Delta f(z)/\langle I_t(z) \rangle$ measurements. In Sec. IV B, we discuss the signal-to-noise ratio in constant height AFM/STM images. In Sec. IV C, we show the AFM/STM images exhibiting double tip features. Finally, our concluding remarks are presented in Sec. V.

II. CONVERSION FORMULAS

In AFM/STM, a cantilever is oscillated and Δf and $\langle I_t \rangle$ are simultaneously measured. STM to measure $\langle I_t \rangle$ between the sample and an oscillating tip is termed dynamic STM, in contrast to conventional static STM. The observables of dynamic AFM/STM, i.e., Δf and $\langle I_t \rangle$, can be described as

$$\Delta f(z) = \frac{f_0}{\pi k A} \int_{-1}^{1} F[z + A(1+u)] \left(\frac{-u}{\sqrt{1-u^2}} \right) du \tag{1}$$

and

$$\langle I_t(z) \rangle = \frac{1}{\pi} \int_{-1}^{1} I_t[z + A(1+u)] \left(\frac{1}{\sqrt{1-u^2}} \right) du, \tag{2}$$

where k, A, and z are the spring constant, the oscillation amplitude of the cantilever, and the distance of closest approach between the tip and sample, respectively.[16–20] Δf ($\langle I_t \rangle$) is calculated by the weighted average of F (I_t) over the tip oscillation from the closest point to the surface ($u=-1$) to the farthest point from the surface ($u=1$).

If the cantilever is oscillated with a tiny amplitude, these formulas can be transformed into simpler forms,

$$\Delta f(z) = -\frac{f_0}{2k} \frac{dF(z)}{dz} \tag{3}$$

and

$$\langle I_t(z) \rangle = I_t(z + A) \tag{4}$$

by substituting $F[z+A(1+u)]=F(z+A)+dF(z)/dz \times Au$ and $I_t[z+A(1+u)]=I_t(z+A)+dI_t(z)/dz \times Au$ into Eqs. (1) and (2), respectively. Δf becomes proportional to the force gradient while $\langle I_t \rangle$ becomes the same as I_t at the tip position of the center of the cantilever oscillation. These small amplitude approximations hold at small A such that $dF(z)/dz$ $[dI_t(z)/dz]$ is kept constant during the cantilever swing. At this small A limit, the interpretation of the topographic image is simple: the topography for maintaining Δf ($\langle I_t \rangle$) constant corresponds to the constant force gradient (tunneling current) surface.

In contrast, at larger A, the interpretation of topography is not simple,[19,21] and Eqs. (3) and (4) are no longer valid. Nevertheless, useful formulas are available for a large A limit. Under a large A limit, Eqs. (1) and (2) can be transformed into the approximation formulas,[16–19]

$$\Delta f(z) = \frac{f_0}{kA^{1.5}} \frac{1}{\sqrt{2}\pi} \int_z^{\infty} \left[\frac{F(z')}{\sqrt{z'-z}} \right] dz' \tag{5}$$

and

$$\langle I_t(z) \rangle = \frac{1}{\sqrt{2A}\pi} \int_z^{\infty} \left[\frac{I_t(z')}{\sqrt{z'-z}} \right] dz'. \tag{6}$$

These large amplitude approximations hold at large A such that F (I_t) becomes zero at the farthest point of the tip from the surface during cantilever swing. Note that the required values of A are different in Eqs. (5) and (6). Equation (6) holds even at much smaller A than that for Eq. (5), because I_t does not include the long-range part whereas F includes it, such as the van der Waals force and the electrostatic force. Using sharp tips such as microfabricated cantilevers, the safe value of A for the large amplitude approximation is 10 nm for dynamic AFM, while 1 nm is sufficient for dynamic STM. Using a blunter tip, a larger A is required for a large A approximation in AFM whereas this is not the case in dynamic STM.

The observables of AFM/STM, i.e., Δf and $\langle I_t \rangle$, can be converted into physical quantities of interest, i.e., F and I_t. F can be derived from $\Delta f(z)$ measurements, which is termed dynamic force spectroscopy.[22–25] I_t can also be numerically deduced from the measured $\langle I_t(z) \rangle$ curve. Hereafter, I_t is the tunneling current at closest separation between the oscillating tip and the surface. This I_t is comparable to the tunneling current observed in conventional static STM. In Eqs. (5) and (6), $\Delta f(z)$ and $\langle I_t(z) \rangle$ are expressed as a function of $F(z)$ and $I_t(z)$. Since both Eqs. (5) and (6) correspond to Abelian integral equations, they can be inversely transformed into the formulas shown below,

$$F(z) = -\frac{kA^{1.5}}{f_0} \sqrt{2} \int_z^{\infty} \left[\frac{d\Delta f(z')/dz'}{\sqrt{z'-z}} \right] dz' \tag{7}$$

and

$$I_t(z) = -\sqrt{2A} \int_z^{\infty} \left[\frac{d\langle I_t(z') \rangle/dz'}{\sqrt{z'-z}} \right] dz', \tag{8}$$

Refs. 17 and 18.

If $I_t(z)$ has exponential distance dependence with a decay constant of κ, $I_t(z)=I_t(0) \times \exp(-\kappa z)$, Eq. (8) can be transformed into the simple formula, $I_t(z)=\langle I_t(z) \rangle \times \sqrt{2\pi\kappa A}$.[19] Nevertheless, since the distance dependence of $I_t(z)$ deviates from the exponential at close distance on the Si(111)-(7 $\times$7) surface as shown below, Eq. (8) should be used for the conversion.

Accurate estimation of A is important for proper conversion of Δf ($\langle I_t \rangle$) to F (I_t). In AFM/STM experiments, A can be precisely measured by using a normalized time-averaged

tunneling current ($\langle I_t \rangle \times \sqrt{A}$), which is independent of A, see Eq. (6), as below. First, the lateral tip position is fixed above a certain site with the tip-surface distance regulated by $\langle I_t \rangle$. Then, A is slightly decreased by changing the set point of A regulation and the $\langle I_t \rangle$ set point is changed such that $\langle I_t \rangle \times \sqrt{A}$ is maintained. The tip-surface feedback system moves the sample toward the oscillating tip by the distance corresponding to the reduced A. Thus, the value of A can be estimated. Since I_t has no long-range part and has strong tip-surface distance dependence, this method can be applied at much smaller A than the gamma method,[26] which has been widely used in noncontact AFM for calibration of A.[16,27] The present method is especially effective using blunter tips because a large A approximation for STM, Eq. (6), still holds. The $I_t(z)$ curve in Fig. 3(b) shows that this new calibration method works even at $A \sim 5$ Å.

III. EXPERIMENTAL

We used a custom-built AFM/STM operated at room temperature and equipped with an optical interferometer as the cantilever deflection sensor. We used a commercial digital scanning probe microscope controller (Dulcinea, Nanotec, S. L., Madrid, Spain) (Ref. 28) for data acquisition of the constant height imaging and the distance spectroscopy. We removed possible contamination on the tip apex of commercially obtained Pt-Ir-coated Si cantilevers (NCLPt/NCHPt, NanoWorld AG, Neuchatel, Switzerland) by Ar-ion sputtering in ultrahigh vacuum. The sputtering condition used is crucial for detecting Δf and $\langle I_t \rangle$ reproducibly. The cantilevers were oscillated in the constant amplitude mode by phase-locked-loop-based commercial electronics (easyPLL plus detector and controller, Nanosurf, Liestal, Switzerland). Since the typical spring constant is 20 N/m, cantilevers are oscillated at a large amplitude, typically 200 Å, for stable cantilever oscillation even at close tip-surface distance.[29] We used Sb-doped Si(111) substrates for sample, whose resistivity is 0.01 Ω cm. The Si(111)-(7×7) reconstructed surfaces were prepared by the standard method of flashing and annealing the samples. V_s was applied to the sample with respect to the grounded tip and $\langle I_t \rangle$ was detected from the tip using a home-built current-to-voltage converter. Simultaneous imaging of Δf and $\langle I_t \rangle$ were carried out by tip scanning on the surface at constant height without feedback for maintaining the tip-surface distance. Thermal drift between the tip and sample was compensated in three dimensions by using atom tracking and feed-forward techniques.[24,30]

IV. RESULTS AND DISCUSSION

A. Tip-surface distance dependence of AFM/STM images

We simultaneously obtained constant height AFM/STM images at $V_s = -200$ mV. The $\langle I_t \rangle$ and Δf images are shown in the left and right columns in Fig. 2, respectively. These images were obtained at various tip-surface distances. The tip-surface distance increased in the order of [(a), (b)]–[(k), (l)]. The same surface area on the Si(111)-(7×7) surface was imaged with the same tip state. Larger absolute values of both Δf and $\langle I_t \rangle$ are expressed as brighter contrasts in Fig. 2.

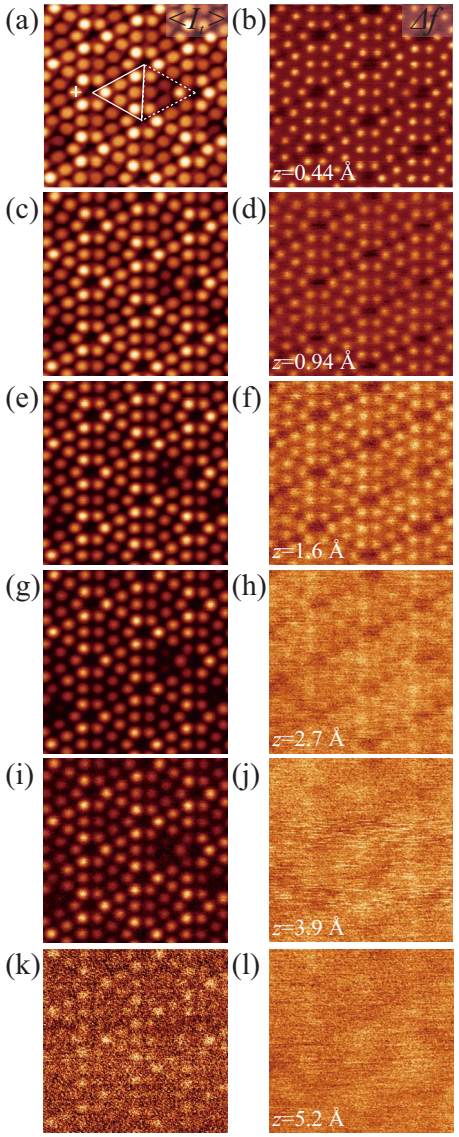

FIG. 2. (Color online) The tip-surface distance dependence of the constant height $\langle I_t \rangle$ and Δf images obtained simultaneously. The images in the left column are $\langle I_t \rangle$ and those in the right column are Δf. The relative tip-surface distances, whose origin is defined in Fig. 3, are shown in the Δf images. The acquisition parameters are $f_0 = 149\,996.3$ Hz, $A = 200$ Å, $k = 22.1$ N/m, $Q = 21\,000$, and $V_s = -200$ mV ($V_{CPD} = -330$ mV), respectively.

The atomic contrast is different for AFM and STM because of the different imaging mechanisms involved.[12,14,15] The $\langle I_t \rangle$ images clearly show the 12 adatoms in each diamond-shaped 7×7 unit cell. The solid (dotted) triangle in Fig. 2(a) corresponds to a faulted (unfaulted) half unit cell. The $\langle I_t \rangle$ images are similar to typical filled state images obtained by conventional STM.[31–33] Corner adatoms look brighter than center adatoms in a half unit cell. The corner (center) adatoms in a faulted half are brighter than corner (center) adatoms in an unfaulted half unit cell. On the other hand, in AFM images, Si adatoms have almost the same contrast except for the slight contrast difference between faulted and unfaulted half unit cells as shown in Figs. 2(b), 2(d), and 2(f). This is the same as the contrast that we have

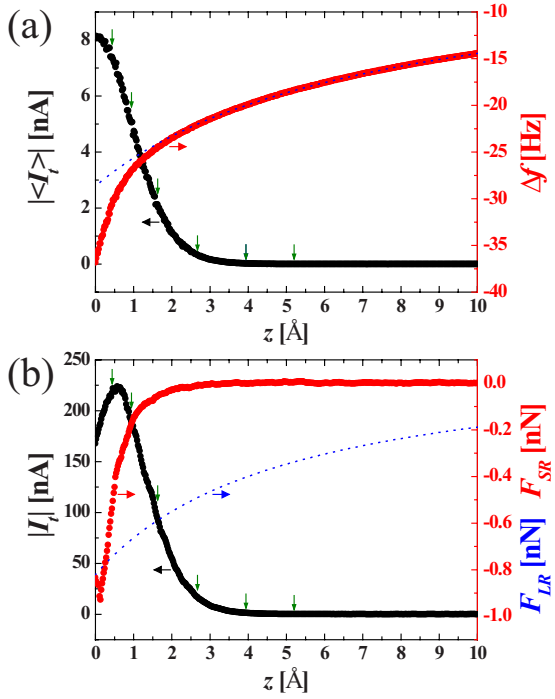

FIG. 3. (Color online) Results of the force/current distance spectroscopy. (a) $\Delta f(z)$ and $\langle I_t(z) \rangle$ curves obtained above the corner adatom in the unfaulted half indicated by the cross in Fig. 2(a). Six sets of curves were averaged. The dotted curve is the fitted $\Delta f_{LR}(z)$ curve. (b) Numerically converted $F_{SR}(z)$, $F_{LR}(z)$, and $I_t(z)$ curves. The vertical arrows indicate the tip-surface distances corresponding to the images in Fig. 2. The acquisition parameters and the tip apex state are the same as those in Fig. 2.

mainly obtained in our AFM topographic images using Si cantilevers.[24,30] There are some unknown defects in this area. In STM, these defects are clearly observed as dark contrast while it is difficult to identify them in AFM. It is expected that the electronic states near the Fermi level are modified around the defect sites.

The atomic contrast is gradually lost with increasing tip-surface distance in both AFM and STM. More importantly, we find that STM can resolve atoms at larger tip-surface distances than AFM. In Figs. 2(i) and 2(j), the STM image clearly shows atomic contrast while atomic resolution is lost in AFM. To estimate the relative tip-surface distances as well as the values of F and I_t on the adatom site for each image in Fig. 2, we carried out point force/current spectroscopy. The $\Delta f(z)$ and $\langle I_t(z) \rangle$ curves were simultaneously measured as shown in Fig. 3(a). The atom tracking technique was applied in the same way as the force spectroscopy previously proposed.[24] These curves were acquired on the corner adatom indicated by the cross in Fig. 2(a). The spectroscopic measurements were performed using the same tip state as that used for imaging. In this paper, the origin of z ($z=0$) is defined as the closest point to the surface in the data acquisition.

The F measured by AFM has two components, i.e., site-independent long-range force (F_{LR}) and site-dependent short-range force (F_{SR}). F_{SR} is a quantity of interest, i.e., the chemical-bonding force between the tip apex atoms and individual surface atoms, which offers atomic resolution in AFM.[34] On the other hand, F_{LR} is a background force acting on the tip at a relatively far distance from the surface, such as van der Waals force and electrostatic force.[35] The F_{LR}-dominant region of the $\Delta f(z)$ curve, which we defined as $z > 3.0$ Å, was fitted into the inverse-power function of z^{-s}.[36] The fitting curve, i.e., the long-range part of $\Delta f(z)$ [$\Delta f_{LR}(z)$] is shown by the dotted curve in Fig. 3(a). For the best fit, $s = 0.70$ was obtained, which corresponds to the $z^{-1.2}$ dependence of $F_{LR}(z)$.[19] This dependence is close to our previous result obtained by the same method.[15] The short-range part of $\Delta f(z)$ [$\Delta f_{SR}(z)$] was obtained by the subtraction of $\Delta f_{LR}(z)$ from the $\Delta f(z)$ curve. Then, the $F_{SR}(z)$ curve was numerically converted from $\Delta f_{SR}(z)$ using Sader's algorithm.[37] The same result was also obtained by using Eq. (7) because of large A. The $\langle I_t(z) \rangle$ curve was converted into the $I_t(z)$ curve using Eq. (8). The derived $F_{SR}(z)$ and $I_t(z)$ curves as well as $F_{LR}(z)$ calculated from the $\Delta f_{LR}(z)$ curve are shown in Fig. 3(b). $\langle I_t \rangle$ and I_t at six different tip-surface distances corresponding to the images in Fig. 2 are indicated by the vertical arrows in Figs. 3(a) and 3(b). We can estimate the values of z, $\langle I_t \rangle$, I_t, Δf, Δf_{SR}, Δf_{LR}, F_{SR}, and F_{LR} on the adatom site at each distance in Fig. 2. These values are summarized in Table I.

Our results clearly show that the tip-surface distance to obtain atomic resolution on the Si(111)-(7×7) surface by AFM is smaller than that in conventional STM. A few hundred piconewton of F_{SR} is detected at $z = 0.44-0.94$ Å, where AFM clearly resolves atoms, Figs. 2(b) and 2(d). These values are in good agreement with the previous value

TABLE I. Various values on the corner adatom for each image in Fig. 2. The values were estimated from Fig. 3.

Image	(a), (b)	(c), (d)	(e), (f)	(g), (h)	(i), (j)	(k), (l)
z (Å)	0.44	0.94	1.6	2.7	3.9	5.2
$\langle I_t \rangle$ (nA)	7.4	5.0	2.1	0.34	0.023	0.001
I_t (nA)	220	190	95	17	1.3	0.034
Δf (Hz)	−30.6	−27.0	−24.5	−22.1	−20.0	−18.4
Δf_{SR} (Hz)	−3.4	−1.2	−0.36	−0.09	0	0
Δf_{LR} (Hz)	−27.2	−25.8	−24.1	−22.0	−20.0	−18.4
F_{SR} (nN)	−0.54	−0.18	−0.057	−0.014	0	0
F_{LR} (nN)	−0.74	−0.67	−0.59	−0.49	−0.40	−0.34

(F_{SR}=150 pN) for obtaining clear AFM topography on the same surface estimated by force spectroscopy using Si cantilevers.[38] At this distance range (z=0.44–0.94 Å), I_t of about 200 nA is observed, which is much greater than typical values for imaging this surface by conventional STM (about 1 nA or less).[31–33] In addition, Fig. 3(b) shows that $I_t(z)$ is deviated from the monotonic exponential distance dependence and even decreases at close tip-surface distances (z <0.6 Å). This is due to chemical-bond formation between tip apex atoms and sample atoms as previously reported.[15,39,40]

At z=3.9 Å, atomic resolution is lost in AFM, Fig. 2(j), while STM still resolves atoms clearly, Fig. 2(i). At this far distance, I_t=1.3 nA was detected, which is close to the typical value for conventional STM. F_{SR} is as small as our minimum detectable force (a few piconewton). At z=5.2 Å, not only Δf but also $\langle I_t \rangle$ images do not show clear atomic contrast. In Fig. 2(k), the corrugation in $\langle I_t \rangle$ is comparable with the minimum detectable current of our current-to-voltage converter (1 pA). Since I_t=34 pA is obtained at this distance, we predict that static STM can resolve atoms even at z=5.2 Å with the same quality as Fig. 2(i). Note that $\langle I_t \rangle$ in Fig. 2(i) is close to I_t in Fig. 2(k). Our systematic experiments clearly demonstrate that the optimal imaging distance is different for AFM and conventional STM. The distance in Figs. 2(b) and 2(d) is the required distance for AFM for clear atomic resolution, whereas the distance in Figs. 2(i) and 2(k) is the typical distance in conventional STM. This difference in the optimal distance is as large as 3–4 Å.

The difference in optimal tip-surface distance between AFM and conventional STM explains our experience that the tip state and/or surfaces are more frequently modified during AFM topographic scanning than in STM operation. For example, it was more difficult to obtain atomic resolution in Si(100)-(1×2) images without permanent modification of the surface by AFM than using conventional static STM.[41] From a different point of view, the necessity for closer approach of a tip to a surface during AFM operation let us notice the movement of atoms strongly bound to semiconductor surfaces. These findings led us to sophisticated mechanical atom manipulations at room temperature[38,42,43] that could not be achieved by STM.

B. Consideration of the signal-to-noise ratio in constant height AFM/STM images

The difference in the tip-surface distance between AFM and STM, where atomic resolution is lost in constant height imaging, can be attributed to the different origins of the signal and noise in their observables. The noise in an AFM topographic image has been previously discussed by Giessibl *et al.*[44] Here, we discuss the signal-to-noise ratio in constant height AFM /STM images. $(S/N)_{\mathrm{AFM}}$ and $(S/N)_{\mathrm{STM}}$ can be written as

$$(S/N)_{\mathrm{AFM}} = \frac{|\Delta f_{SR}(z)|}{\sqrt{\delta\Delta f_{therm.}^2 + \delta\Delta f_{det.}^2 + \delta\Delta f(z)_{mecha.}^2}} \tag{9}$$

and

$$(S/N)_{\mathrm{STM}} = \frac{|\langle I_t(z)\rangle|}{\sqrt{\delta\langle I_t\rangle_{det.}^2 + \delta\langle I_t(z)\rangle_{mecha.}^2}}, \tag{10}$$

where $\delta\Delta f_{therm.}$ is thermal noise, $\delta\Delta f_{det.}$ ($\delta\langle I_t\rangle_{det.}$) is the detector noise, and $\delta\Delta f(z)_{mecha.}$ ($\delta\langle I_t(z)\rangle_{mecha.}$) is mechanical noise. These different sources of noise are statistically independent. Note that only $\Delta f_{SR}(z)$ contributes to atomic contrast in constant height AFM as the signal while $\Delta f_{LR}(z)$ just contributes to the background.[15] $\delta\Delta f_{therm.}$ originates in thermal fluctuations of the cantilever and is written as $\delta\Delta f_{therm.} = \sqrt{k_B T B f_0 / k A^2 \pi Q}$, where $k_B T$, B, and Q are the thermal energy, the bandwidth of the frequency demodulator, and the quality factor of the cantilever, respectively.[2] $\delta\Delta f_{det.}$ originates in the noise density of the cantilever deflection sensor (n) and is written as $\delta\Delta f_{det.} = nB^{1.5}/\pi A$.[2] $\delta\langle I_t\rangle_{det.}$ originates in the noise density in the preamplifier for current detection (n') and is written as $\delta\langle I_t\rangle_{det.} = n'\sqrt{B'}$ using the bandwidth for the current detector (B').[2] $\delta\Delta f(z)_{mecha.}$ and $\delta\langle I_t(z)\rangle_{mecha.}$ originate in the fluctuation of the gap between the tip and surface due to the mechanical noise in the microscope, including external vibrations and acoustic noise. These different types of noise are written in terms of the product of the mechanical noise in the gap ($\delta z_{mecha.}$) and the slope of $\Delta f(z)$ and $\langle I_t(z)\rangle$ with respect to z as $\delta\Delta f(z)_{mecha.} = |d\Delta f(z)/dz| \times \delta z_{mecha.}$ and $\delta\langle I_t(z)\rangle_{mecha.} = |d\langle I_t(z)\rangle/dz| \times \delta z_{mecha.}$. Although $\delta z_{mecha.}$ is independent of z, $\delta\Delta f(z)_{mecha.}$ [$\delta\langle I_t(z)\rangle_{mecha.}$] depends on z. That is, the mechanical noise increases with the slope of $\Delta f(z)$ [$\langle I_t(z)\rangle$].

We estimated the noise in $\Delta f(z)$ [$\langle I_t(z)\rangle$] by analyzing the data shown in Fig. 3(a). The noise in $\Delta f(z)$ [$\langle I_t(z)\rangle$] was evaluated as the difference between the $\Delta f(z)$ [$\langle I_t(z)\rangle$] raw curve and the same curve smoothed using a ten-point window. The z dependence of the noise in $\Delta f(z)$ and $\langle I_t(z)\rangle$ are plotted in Figs. 4(a) and 4(b), respectively. At a far distance, the noise in $\Delta f(z)$ and $\langle I_t(z)\rangle$ is almost independent of z. In this region, $\delta\langle I_t\rangle_{det.}$ ($\delta\Delta f_{therm.}$ and $\delta\Delta f_{det.}$), which is z independent, are dominant in STM (AFM) because $d\langle I_t(z)\rangle/dz$ [$d\Delta f(z)/dz$] is too small to provide significant mechanical noise. At a close distance, the noise becomes larger since the slope of $\Delta f(z)$ and $\langle I_t(z)\rangle$ become larger, wherein the mechanical noise is dominant. This region is fitted into the $\delta\Delta f(z)_{mecha.} = |d\Delta f(z)/dz| \times \delta z_{mecha.}$ and $\delta\langle I_t(z)\rangle_{mecha.} = |d\langle I_t(z)\rangle/dz| \times \delta z_{mecha.}$ as shown by the curves in Fig. 4. $\delta z_{mecha.}$=6 pm was chosen for the best fit and the same value was used in both AFM and STM. $\delta\Delta f(z)_{mecha.}$ and $\delta\langle I_t(z)\rangle_{mecha.}$ fit the noise experimentally obtained at close distance very well. This distance dependence of the noise in $\Delta f(z)$ has also been observed in our previous force spectroscopic measurements, wherein the noise clearly increased with the slope of $\Delta f(z)$.[24,45] The mechanical noise at close distance is also seen not only in dynamic AFM/STM but also static STM (not shown). Therefore, this is not specific to dynamic AFM/STM but is common in scanning probe microscopy.

The signal-to-noise ratio in dynamic AFM [$(S/N)_{\mathrm{AFM}}$] is smaller than that in dynamic STM [$(S/N)_{\mathrm{STM}}$] over the whole distance range. That is easily confirmed by substituting the noise shown in Fig. 4 into the denominators and the signal, i.e., Δf_{SR} and $\langle I_t\rangle$, into the numerators in Eqs. (9) and

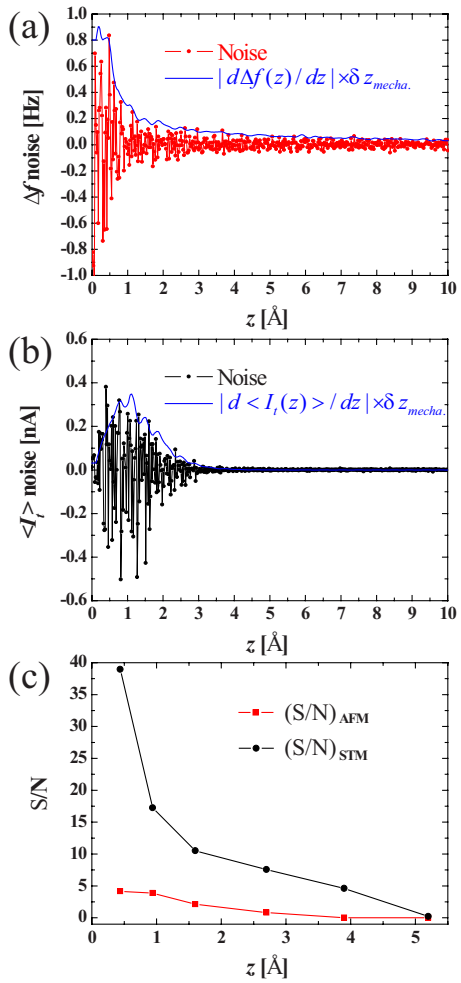

FIG. 4. (Color online) The tip-surface distance dependence of the (a) Δf noise and (b) $\langle I_t\rangle$ noise. The noise is estimated from the single raw curve in Fig. 3(a). The curves for the calculated mechanical noise are indicated in (a) and (b). $\delta z_{mecha.}=6$ pm is chosen for the best fit. (c) The plots of $(S/N)_{\mathrm{AFM}}$ and $(S/N)_{\mathrm{STM}}$ corresponding to the images in Fig. 2.

(10). The $(S/N)_{\mathrm{AFM}}$ and $(S/N)_{\mathrm{STM}}$ at z corresponding to the images in Fig. 2 are plotted in Fig. 4(c). It is shown that STM can yield atomic resolution at larger tip-surface distances than AFM. Note that $(S/N)_{\mathrm{AFM}}<(S/N)_{\mathrm{STM}}$ means the image contrast in AFM is worse than that in STM. When the force field reflects a finer structure on a surface than the tunneling current, the spatial resolution in AFM becomes higher than that in STM.[11,14,46,47]

The image quality at a different distance range is determined by different origins of $(S/N)_{\mathrm{AFM}}$ and $(S/N)_{\mathrm{STM}}$. The distance in Figs. 2(a)–2(f) is the mechanical noise dominant region whereas that in Figs. 2(i)–2(l) is not. We discuss the method to improve the $(S/N)_{\mathrm{AFM}}$ and $(S/N)_{\mathrm{STM}}$ at far and close distances separately. At a far distance, $(S/N)_{\mathrm{AFM}} \approx |\Delta f_{SR}(z)|/\sqrt{\delta\Delta f_{therm.}^2+\delta\Delta f_{det.}^2}$ and $(S/N)_{\mathrm{STM}} \approx |\langle I_t(z)\rangle|/\delta\langle I_t\rangle_{det.}$ are approximately obtained. $(S/N)_{\mathrm{AFM}}$ can be enhanced by improvement of the cantilever deflection sensor. By decreasing n, $(S/N)_{\mathrm{AFM}}$ can be increased until the thermal limit is reached, where $\delta\Delta f_{therm.}$ is the dominant noise source. $(S/N)_{\mathrm{STM}}$ also increases with the reduction in n'.

$(S/N)_{\mathrm{AFM}}$ and $(S/N)_{\mathrm{STM}}$ can be enhanced by decreasing A for the same reason as reported previously.[2,44] At large A approximation, $\Delta f_{SR}(z)$ is proportional to $A^{-1.5}$, see Eq. (5), and $\sqrt{\delta\Delta f_{therm.}^2+\delta\Delta f_{det.}^2}$ is proportional to A^{-1}. On the other hand, $\langle I_t(z)\rangle$ is proportional to $A^{-0.5}$, see Eq. (6), and $\delta\langle I_t\rangle_{det.}$ is independent of A. Thus, both $(S/N)_{\mathrm{AFM}}$ and $(S/N)_{\mathrm{STM}}$ are inversely proportional to $\sqrt{A}$ for a large A range.[2] These can increase with decreasing A from the present parameter ($A \sim 200$ Å). Since $\Delta f_{SR}(z)$ has no A dependence at a small A limit, see Eq. (3), there is an optimal A to obtain maximum $(S/N)_{\mathrm{AFM}}$. Giessibl *et al.*[44] proposed that the optimal A corresponds to the decay length of F, typically $A=1$ Å. On the other hand, $(S/N)_{\mathrm{STM}}$ becomes maximum at the $A=0$ limit since $\langle I_t\rangle$ monotonically increases with decreasing A over the whole range, see Eq. (2).

Nevertheless, to operate AFM/STM at such small A, larger k is required for stable cantilever oscillation.[29] The choice of cantilevers is not straightforward. Decreasing f_0/k reduces $(S/N)_{\mathrm{AFM}}$ since $\Delta f_{SR}(z)$ is proportional to f_0/k, $\delta\Delta f_{therm.}$ is proportional to $\sqrt{f_0/k}$, and $\delta\Delta f_{det.}$ is independent of f_0/k. Therefore, when we choose the value of A, there is a trade-off between high $(S/N)_{\mathrm{AFM}}$ [$(S/N)_{\mathrm{STM}}$] and high stability of the cantilever oscillation.

At close distances, where mechanical noise becomes dominant, $(S/N)_{\mathrm{AFM}} \approx |\Delta f_{SR}(z)|/[|d\Delta f(z)/dz| \times \delta z_{mecha.}]$ and $(S/N)_{\mathrm{STM}} \approx |\langle I_t(z)\rangle|/[|d\langle I_t(z)\rangle/dz| \times \delta z_{mecha.}]$ are approximately obtained. Figure 4 shows that $\delta\Delta f(z)_{mecha.}$ ($\delta\langle I_t(z)\rangle_{mecha.}$) becomes much larger than other noise sources around $z=1$ Å. This distance is the typical distance for AFM imaging. Importantly, in this region, $(S/N)_{\mathrm{AFM}}$ and $(S/N)_{\mathrm{STM}}$ cannot be enhanced by decreasing the noise density of the deflection sensor and current-to-voltage converter. The mechanical stability of the microscope needs to be increased to improve $(S/N)_{\mathrm{AFM}}$ and $(S/N)_{\mathrm{STM}}$.

In this region, the $(S/N)_{\mathrm{AFM}}$ suffers from Δf_{LR} in contrast to the far distance since $\delta\Delta f(z)_{mecha.}$ depends on both long- and short-range contributions. Note that $d\Delta f(z)/dz = d\Delta f_{LR}(z)/dz + d\Delta f_{SR}(z)/dz$. The presence of F_{LR} makes $(S/N)_{\mathrm{AFM}}$ smaller since Δf_{LR} contributes to the mechanical noise in spite of no contribution to the signal. As shown in Fig. 3(b), $|F_{LR}|$ is gradually increased with decreasing tip-surface distance, while $|F_{SR}|$ rapidly increases at $z<2$ Å and reaches the maximum attractive force ($F_{SR}=-0.89$ nN) at $z=0.10$ Å. F_{LR} in this study using Pr-Ir-coated Si cantilevers is much greater than that in previous AFM studies using normal Si cantilevers (NCLR, NanoWorld AG, Neuchatel, Switzerland). The relative strength of F_{LR} with respect to the total F is about 50% at a maximum attractive F_{SR} distance using Pt-Ir-coated Si cantilevers while this is only 10% using normal Si cantilevers.[24,25,45] The tip radius of a Pt-Ir-coated Si cantilever is greater than that of a normal Si cantilever since the tip apex is covered with Pt-Ir with a thickness of about 25 nm. In addition, not only van der Waals force but also a substantial electrostatic force contributes to F_{LR} since the applied V_s deviates from the voltage (V_{CPD}) to minimize the electrostatic force in the present AFM/STM study. Furthermore, Δf_{SR} is much smaller than Δf_{LR} since we operate

the AFM with a large A. Even at the closest distance in the acquisition, Fig. 2(b), Δf_{LR} is eight times as large as Δf_{SR}. Using a sharper tip can decrease F_{LR} and Δf_{LR}, leading to efficient improvement of the $(S/N)_{\mathrm{AFM}}$. One possible way is to coat the normal Si tip with a thin metal layer by evaporation.[48]

In addition, the reduction in A increases the sensitivity of F_{SR} with respect to F_{LR}, which has been proposed by Giessibl.[19,49,50] Here, we show that $(S/N)_{\mathrm{AFM}}$ can be enhanced due to this effect. At a large A limit, $(S/N)_{\mathrm{AFM}}$ does not depend on A because $\Delta f_{SR}(z)$ and $d\Delta f(z)/dz$ have the same A dependence $(A^{-1.5})$. However, with decreasing A, only $d\Delta f(z)/dz$, which includes a long-range component, starts to deviate from the $A^{-1.5}$ dependence and has a weaker A dependence while $\Delta f_{SR}(z)$ still has a $A^{-1.5}$ dependence. Thus, $(S/N)_{\mathrm{AFM}}$ is enhanced until the small A limit is reached.[51] In this limit, $(S/N)_{\mathrm{AFM}}$ is independent of A since $\Delta f_{SR}(z)$ and $d\Delta f(z)/dz$ do not show an A dependence.

To improve the atomic contrast in an AFM image at a mechanical noise dominant distance, the use of a sharp tip and/or small A operation is effective. For small A operation, a cantilever with a larger k is required for the stability of the cantilever oscillation. As far as the mechanical noise is dominant, the decrease in f_0/k does not sacrifice $(S/N)_{\mathrm{AFM}}$ since $(S/N)_{\mathrm{AFM}}$ is independent of f_0/k.

On the other hand, $(S/N)_{\mathrm{STM}}$ does not depend on both the tip sharpness and A at a mechanical noise-dominant distance since $\langle I_t(z)\rangle$ has no long-range part. Assuming $I_t(z)=I_t(0)\times\exp(-\kappa z)$ for simplicity, it can be proven that $(S/N)_{\mathrm{STM}}=1/(\kappa\times\delta z_{mecha.})$, and thus $(S/N)_{\mathrm{STM}}$ has no A dependence over the whole A range. This can explain our experience that it is difficult to obtain atomic resolution in AFM with large A using blunt tips while STM can still resolve atoms using the same tip.

C. AFM/STM images exhibiting double tip features

We note that the difference in the optimal tip-surface distance between AFM and STM influences the contrast in AFM/STM images obtained by double tips. In simultaneous AFM/STM measurements, the imaging area by AFM usually coincides with that by STM as shown in Fig. 2. This indicates that the same front atom on the tip apex plays a role in atomic resolution in both AFM and STM. In contrast, we occasionally obtained anomalous AFM/STM images accounted for by double tips. The $\langle I_t\rangle$ images in Figs. 5(a), 5(c), and 5(e) were simultaneously obtained with the Δf images of Figs. 5(b), 5(d), and 5(f), respectively. These were obtained at a constant height scan. The STM image in Fig. 5(a) shows a double tip feature as previously reported.[52,53] This image looks like a superposition of two 7×7 adatom patterns as indicated by the dotted and solid rhombuses. The position of the solid rhombus is laterally shifted from the dotted rhombus by 8.3 Å. On the other hand, the AFM image obtained simultaneously does not show the double tip feature. The 7×7 pattern in Fig. 5(b) coincides with one of the patterns in Fig. 5(a). The common unit cell is indicated by the dotted rhombus. Note that these anomalous images were sometimes obtained and normal contrast in AFM/STM

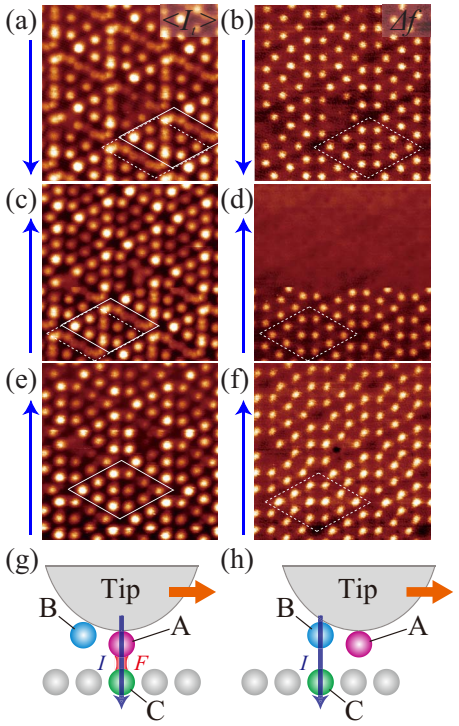

FIG. 5. (Color online) [(a)–(f)] Constant height $\langle I_t\rangle$ and Δf images showing double tip features. The $\langle I_t\rangle$ images [(a), (c), and (e)] were obtained simultaneously with the Δf images [(b), (d), and (f)], respectively. The slow scan directions are indicated by the arrows. The acquisition parameters are $f_0=145\,968.8$ Hz, $A=214$ Å, $k=20.4$ N/m, $Q=27\,000$, and $V_s=-400$ mV ($V_{CPD}=-549$ mV). [(g) and (h)] A schematic model to explain the images.

can be easily recovered by soft contact between the tip and sample.

One possible model to explain these images is sketched out in the schematic drawings in Figs. 5(g) and 5(h). Here, two atoms A and B are located on the tip apex with a lateral interval of 8.3 Å. Atom A is located at the nearest neighbor from the surface and atom B is at the second-nearest neighbor. When atom A is located above atom C on the surface, see Fig. 5(g), atom A interacts with atom C forming atomic contrast in the AFM image. At the same time, the tunneling current flows between atom A and atom C providing an STM signal. When atom B is located above atom C, see Fig. 5(h), after tip scanning at constant height, the tunneling current now flows between them. Atom B does not contribute to the AFM image if the distance between atoms B and C is not sufficiently small to generate significant interaction. As we have discussed in the previous sections, STM can produce atomic contrast with the tip located farther away from the surface compared to AFM. Thus, an STM image shows double tip features produced by atoms A and B, while an AFM image does not, with only atom A contributing to the atomic resolution.

After obtaining the images in Figs. 5(a) and 5(b), we successively acquired the images in Figs. 5(c) and 5(d). The slow scan direction is from the bottom to the top. The lower part of the images in Figs. 5(c) and 5(d) reproduce Figs. 5(a) and 5(b). After that, the tip change occurred leading to a

contrast change. The STM image changed from double tip contrast to normal contrast while atomic contrast was lost in the AFM image. Using the above model, this can be explained by the displacement of only atom A on the tip while maintaining the position of atom B. The 7×7 pattern in STM produced by atom B is not changed. The value of $\langle I_t \rangle$ on corner adatoms in unfaulted half unit cells is estimated to be 0.75 nA in the upper part of Fig. 5(c). This supports the idea that atom B is not sufficiently close to the surface to form a strong chemical bond.

We obtained different types of AFM/STM images at $V_s = -400$ mV, which cannot be explained by the model above, as shown in Figs. 5(e) and 5(f). In these, although the atomic contrast in both AFM and STM looks normal, the 7×7 patterns do not coincide in the AFM and STM images. By using the defects seen in these images as markers, we can identify the same unit cell as indicated by the rhombuses. The solid rhombus in STM and the dotted rhombus in AFM are laterally deviated by 8.5 Å. The tip apex atom for AFM imaging and that for STM imaging should be different. The atom that plays a role in AFM imaging does not mediate the tunneling current while the atom for STM imaging does not contribute to atomic contrast in AFM. Although the imaging mechanism has not been understood, this effect could be attributed to the electronic state of the tip apex atoms.[53] AFM/STM simultaneous measurements can give more information about the tip structure and electronic state than single AFM or STM operation. These results indicate that tip apex atoms that mediate the tunneling current cannot be identified only by AFM operation.

V. SUMMARY

We have elucidated the tip-surface distance dependence of AFM/STM images on the Si(111)-(7×7) surface by combining constant height imaging and point distance spectroscopy. It was experimentally proved that the tip-surface distance for AFM imaging is smaller than that for conventional static STM imaging by 3–4 Å. Therefore, I_t at the distance where AFM clearly resolves atoms is much larger than typical values in conventional STM. On the other hand, F_{SR} is too small to provide AFM contrast at conventional distances for static STM. At close distances, chemical-bond formation between tip apex atoms and sample atoms contributes not only to atomic resolution in AFM but also to the current drop in STM. At far distances, the surface can be imaged by STM without mechanical perturbations due to the tip-surface interaction. It was shown that the difference in the optimal distances between AFM and STM originated in the difference in the signal-to-noise ratio in constant height images. $(S/N)_{\mathrm{AFM}}$ is smaller than $(S/N)_{\mathrm{STM}}$ over the whole tip-surface distance range. We showed that the tip-surface distance can be divided into two parts, i.e., mechanical noise dominant region (close distance) and nondominant region (far distance). At far distances, both $(S/N)_{\mathrm{AFM}}$ and $(S/N)_{\mathrm{STM}}$ increase with decreasing A due to the property of the observables in AFM/STM. At close distances, only $(S/N)_{\mathrm{AFM}}$ increases with decreasing A due to enhancement of the sensitivity of F_{SR} to F_{LR}. In addition, double tip effects that appear in AFM/STM images are shown, suggesting the possibility of characterization of the tip apex.

ACKNOWLEDGMENTS

This work was supported by a Grant-in-Aid for Scientific Research (Grants No. 19053006, No. 17101003, No. 21246010, No. 21656013, and No. 20760024) from the Ministry of Education, Culture, Sports, Science and Technology of Japan (MEXT), Japan Science and Technology Agency (JST), Handai FRC, The project Atomic Technology funded by MEXT and Global COE programs. The work of Y.S. is supported by The Frontier Research Base for Global Young Researchers, Osaka University, in the Program of Promotion of Environmental Improvement to Enhance Young Researchers Independence under the Special Coordination Funds for Promoting Science and Technology of MEXT.

*ysugimoto@afm.eei.eng.osaka-u.ac.jp

[1] *Noncontact Atomic Force Microscopy*, edited by S. Morita, R. Wiesendanger, and E. Meyer (Springer-Verlag, Berlin, 2002).
[2] F. J. Giessibl, Rev. Mod. Phys. **75**, 949 (2003).
[3] T. R. Albrecht, P. Grütter, D. Horne, and D. Rugar, J. Appl. Phys. **69**, 668 (1991).
[4] *Noncontact Atomic Force Microscopy*, edited by S. Morita, F. J. Giessibl, and R. Wiesendanger (Springer-Verlag, Berlin, 2009), Vol. 2.
[5] T. Arai and M. Tomitori, Jpn. J. Appl. Phys., Part 1 **39**, 3753 (2000).
[6] G. H. Enevoldsen, H. P. Pinto, A. S. Foster, M. C. R. Jensen, A. Kuhnle, M. Reichling, W. A. Hofer, J. V. Lauritsen, and F. Besenbacher, Phys. Rev. B **78**, 045416 (2008).
[7] A. Oral, R. A. Grimble, H. O. Ozer, and J. B. Pethica, Rev. Sci. Instrum. **74**, 3656 (2003).
[8] C. Loppacher, M. Bammerlin, M. Guggisberg, S. Schar, R. Bennewitz, A. Baratoff, E. Meyer, and H.-J. Guntherodt, Phys. Rev. B **62**, 16944 (2000).
[9] M. Guggisberg, M. Bammerlin, R. Luthi, C. Loppacher, F. Battiston, J. Lu, A. Baratoff, E. Meyer, and H. J. Guntherodt, Appl. Phys. A **66**, S245 (1998).
[10] P. Güthner, J. Vac. Sci. Technol. B **14**, 2428 (1996).
[11] S. Hembacher, F. J. Giessibl, and J. Mannhart, Science **305**, 380 (2004).
[12] S. Hembacher, F. J. Giessibl, J. Mannhart, and C. F. Quate, Phys. Rev. Lett. **94**, 056101 (2005).
[13] M. Ternes, C. P. Lutz, C. F. Hirjibehedin, F. J. Giessibl, and A. J. Heinrich, Science **319**, 1066 (2008).
[14] L. Gross, F. Mohn, N. Moll, P. Liljeroth, and G. Meyer, Science **325**, 1110 (2009).
[15] D. Sawada, Y. Sugimoto, K. Morita, M. Abe, and S. Morita, Appl. Phys. Lett. **94**, 173117 (2009).
[16] F. J. Giessibl, Phys. Rev. B **56**, 16010 (1997).

[17] U. Dürig, Appl. Phys. Lett. **75**, 433 (1999).
[18] U. Dürig, Appl. Phys. Lett. **76**, 1203 (2000).
[19] F. J. Giessibl and H. Bielefeldt, Phys. Rev. B **61**, 9968 (2000).
[20] F. J. Giessibl, Appl. Phys. Lett. **78**, 123 (2001).
[21] Y. Sugimoto, T. Namikawa, K. Miki, M. Abe, and S. Morita, Phys. Rev. B **77**, 195424 (2008).
[22] H. Hölscher, A. Schwarz, W. Allers, U. D. Schwarz, and R. Wiesendanger, Phys. Rev. B **61**, 12678 (2000).
[23] M. A. Lantz, H. J. Hug, R. Hoffmann, P. J. A. van Schendel, P. Kappenberger, S. Martin, A. Baratoff, and H. J. Guntherodt, Science **291**, 2580 (2001).
[24] M. Abe, Y. Sugimoto, O. Custance, and S. Morita, Appl. Phys. Lett. **87**, 173503 (2005).
[25] Y. Sugimoto, P. Pou, M. Abe, P. Jelinek, R. Perez, S. Morita, and O. Custance, Nature (London) **446**, 64 (2007).
[26] In the gamma method, the tip-surface distance is regulated by Δf and normalized frequency shift ($\gamma = \Delta f k A^{1.5}/f_0$) is kept constant in the calibration.
[27] F. J. Giessibl, Appl. Phys. Lett. **76**, 1470 (2000).
[28] I. Horcas, R. Fernandez, J. Gomez-Rodriguez, J. Colchero, J. Gomez-Herrero, and A. Baro, Rev. Sci. Instrum. **78**, 013705 (2007).
[29] F. J. Giessibl, S. Hembacher, M. Herz, C. Schiller, and J. Mannhart, Nanotechnology **15**, S79 (2004).
[30] M. Abe, Y. Sugimoto, T. Namikawa, K. Morita, N. Oyabu, and S. Morita, Appl. Phys. Lett. **90**, 203103 (2007).
[31] R. M. Tromp, R. J. Hamers, and J. E. Demuth, Phys. Rev. B **34**, 1388 (1986).
[32] P. Avouris and R. Wolkow, Phys. Rev. B **39**, 5091 (1989).
[33] O. Paz, I. Brihuega, J. M. Gomez-Rodriguez, and J. M. Soler, Phys. Rev. Lett. **94**, 056103 (2005).
[34] R. Pérez, M. C. Payne, I. Štich, and K. Terakura, Phys. Rev. Lett. **78**, 678 (1997).
[35] M. Guggisberg, M. Bammerlin, C. Loppacher, O. Pfeiffer, A. Abdurixit, V. Barwich, R. Bennewitz, A. Baratoff, E. Meyer, and H.-J. Guntherodt, Phys. Rev. B **61**, 11151 (2000).
[36] Precisely, van der Waals force and electrostatic force should be treated independently by measuring $\Delta f - V_s$ at every z point (Ref. 35). Therefore, this fitting method may produce some errors in F_{SR} values. We will discuss this issue elsewhere.
[37] J. E. Sader and S. P. Jarvis, Appl. Phys. Lett. **84**, 1801 (2004).
[38] Y. Sugimoto, P. Jelinek, P. Pou, M. Abe, S. Morita, R. Perez, and O. Custance, Phys. Rev. Lett. **98**, 106104 (2007).
[39] P. Jelínek, M. Švec, P. Pou, R. Perez, and V. Cháb, Phys. Rev. Lett. **101**, 176101 (2008).
[40] D. Sawada, Y. Sugimoto, K. Morita, M. Abe, and S. Morita, J. Vac. Sci. Technol. B **28**, C4D1 (2010).
[41] D. Sawada, T. Namikawa, M. Hiragaki, Y. Sugimoto, M. Abe, and S. Morita, Jpn. J. Appl. Phys. **47**, 6085 (2008).
[42] Y. Sugimoto, M. Abe, S. Hirayama, N. Oyabu, O. Custance, and S. Morita, Nature Mater. **4**, 156 (2005).
[43] Y. Sugimoto, P. Pou, O. Custance, P. Jelinek, M. Abe, R. Perez, and S. Morita, Science **322**, 413 (2008).
[44] F. J. Giessibl, H. Bielefeldt, S. Hembacher, and J. Mannhart, Appl. Surf. Sci. **140**, 352 (1999).
[45] Y. Sugimoto, S. Innami, M. Abe, O. Custance, and S. Morita, Appl. Phys. Lett. **91**, 093120 (2007).
[46] T. Eguchi *et al.*, Phys. Rev. Lett. **93**, 266102 (2004).
[47] Y. Sugimoto, M. Abe, S. Hirayama, and S. Morita, Nanotechnology **17**, 4235 (2006).
[48] Y. Naitoh, Y. Kinoshita, Y. J. Li, M. Kageshima, and Y. Sugawara, Nanotechnology **20**, 264011 (2009).
[49] F. J. Giessibl, S. Hembacher, H. Bielefeldt, and J. Mannhart, Science **289**, 422 (2000).
[50] F. J. Giessibl, H. Bielefeldt, S. Hembacher, and J. Mannhart, Ann. Phys. **10**, 887 (2001).
[51] Y. Sugimoto *et al.* (unpublished).
[52] S. I. Park, J. Nogami, and C. F. Quate, Phys. Rev. B **36**, 2863 (1987).
[53] S. I. Park, J. Nogami, H. A. Mizes, and C. F. Quate, Phys. Rev. B **38**, 4269 (1988).